Synergic strategies to improve the PBF-LB/M processability of a cracking-sensitive alloy

Materials & Design 224 (2022) 111396

Contents lists available at ScienceDirect

Materials & Design

journal homepage: www.elsevier.com/locate/matdes

Synergic strategies to improve the PBF-LB\M processability of a cracking-sensitive alloy

A Martucci [a,*], A Aversa [a,b], F Bondioli [a,b], P Fino [a], M Lombardi [a,b]

[a] Department of Applied Science and Technology, Politecnico di Torino, Corso Duca degli Abruzzi 24, 10129 Turin, Italy
[b] Consorzio Interuniversitario Nazionale per la Scienza e Tecnologia dei Materiali (INSTM), Via G. Giusti 9, 50121 Firenze, Italy

HIGHLIGHTS

- A tailored AlSi10Cu8Mg composition was selected to define strategies to process cracking-sensitive compositions via PBF-LB\M.
- After the first process trial, undesirable and harmful delaminations were found.
- An accurate study of residual stress formation enabled the most sensitive parameters to be determined.
- No platform heating was exploited.
- The synergetic use of appropriate process parameters and support structures led to crack-free and fully dense specimens.

GRAPHICAL ABSTRACT

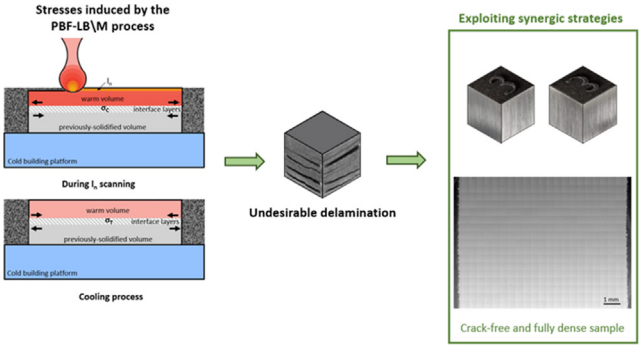

ARTICLE INFO

Article history:
Received 25 August 2022
Revised 3 November 2022
Accepted 18 November 2022
Available online 21 November 2022

Keywords:
Processability
Cracking-sensitive alloy
Aluminium alloys
Residual stresses
Support structures
Process parameters
PBF-LB\M

ABSTRACT

The Powder Bed Fusion-Laser Beam\Metals (PBF-LB\M) is a promising additive manufacturing process that can be used to directly produce functional components with a complex shape for a wide variety of applications. However, the layer-by-layer scanning and high cooling rates result in a high thermal gradient and thus, in thermally induced stresses. The stresses developed during the additive process could lead to undesirable cracking and delamination phenomena that can seriously affect the performance of the final component. The alloy composition can exacerbate crack and delamination formation, however, the need to expand the portfolio of high-strength materials processable for PBF-LB\M makes the resolution of these undesirable phenomena a primary challenge in the additive manufacturing field. This works aims to systematically investigate some strategies to make processable non-standard compositions. As no standard compositions, the promising pre-alloyed AlSi10Cu8Mg composition was chosen for the present work. Based on the results obtained from a condition of severe delamination, the synergetic use of appropriate process parameters and support structures can lead to crack-free and fully dense specimens also when platform heating is not allowed. The developed approach could also be applied to adapt other cracking-sensitive alloys for PBF-LB\M production.

1. Introduction

As one of the best-performing additive manufacturing techniques, Powder Bed Fusion-Laser Beam\Metals (PBF-LB\M) has attracted wide attention in both research and industrial fields. Dur-

* Corresponding author.
E-mail addresses: alessandra.martucci@polito.it (A Martucci), alberta.aversa@polito.it (A Aversa), federica.bondioli@polito.it (F Bondioli), paolo.fino@polito.it (P Fino), mariangela.lombardi@polito.it (M Lombardi).

https://doi.org/10.1016/j.matdes.2022.111396
0264-1275/

ing this advanced process, a high-intensity laser selectively scans successive layers of powder, enabling the production of complex near-*net*-shape parts.

The comparative study conducted by Avateffazeli et al. established that the PBF-LB\M high cooling rates (10^5-10^7 Ks^{-1}) result in finer microstructure, extended solid solubility and facilitated metastable phase formation compared to traditional processes characterised by significantly lower cooling rates (10^1-10^3 Ks^{-1}) [1]. Zhao et al. exploited these PBF-LB\M features to obtain microstructural changes resulting in improved performance of the final component [2]. Furthermore, as investigated by Dadbakhsh and Hao, the PBF-LB\M process facilitates in-situ reaction, allowing the production of advanced metal matrix composites with high hardening properties [3]. However, the extremely rapid cooling rate generates a large quantity of residual stresses on the built component facilitating the formation of delaminations and cracks [4]. In addition, Hyer et al. found that the short time between liquidus and solidus temperature inhibits crack healing by merging grains or liquid backflow, thus facilitating hot tearing [5].

Although the residual stresses can be reduced with different strategies, solving the problem of cracks, delaminations and distortion is complex and not always possible [6]. According to Han et al., although post-processing treatments, such as hot isostatic pressing (HIP) treatment, can substantially aid the processability by PBF-LB\M, these cannot easily delete cracking and delamination effects [7]. To ensure the effectiveness of the HIP treatment, the crack positions and crack morphologies need to be taken into account. In particular, cracks with large widths or exposed to the part surface cannot be fully eliminated with this technology. Based on these considerations, preventing these dangerous phenomena appears advisable. Among the most widely used methods to reduce residual stresses and avoid cracking or delamination, the optimisation of process parameters stands out. The process parameters involved in PBF-LB\M production are numerous, but Jiang et al. found that the ones with the strongest impact on reducing residual stresses and improving the bulk densification are the scanning strategy and the scan speed [8]. According to the pragmatic simulations conducted by Kruth et al., the scan strategies should be optimised by avoiding elevated scan vector lengths and scan vectors uniformly oriented [9]. These shrewdnesses in the scanning strategy result in a beneficial isotropic stress tensor in the component [10]. The described condition can be addressed with the scanning strategy known as the chessboard strategy (or island strategy). The chessboard strategy was exploited by Koutny et al. to drastically reduce the major microstructural defects [11]. In addition, Guo et al. demonstrated that using a chessboard strategy, dense samples with a limited presence of cracks and improved mechanical proprieties can be produced [12]. An important role in processability through PBF-LB\M is played by the volumetric energy density (VED), by its appropriate setting Zhang et al. obtained important benefits on densification and tensioning of the samples [13]. In accordance with Deng et al. work, among the parameters included in the VED calculation, the scanning speed has the strongest effect on the residual stresses and thus crack formation [14]. Levkulich et al. with the reduction of laser scan speed achieved an enhanced densification behaviour during the PBF-LB\M process and a reduced level of residual stresses [15]. Another method widely used to limit the problem correlated to the PBF-LB\M process is represented by the platform preheating [16]. Buchbinder et al. observed that this procedure can be beneficial in slowing down heat flow and cooling rates reducing the development of residual stresses and thus the delamination and crack formation [17]. However, platform heating is not always possible because many lab-scale machines for the PBF-LB\M processing are not equipped with a heating system. In addition for low-melting materials such as aluminium alloys, the temperatures typically used for platform heating result in a heat treatment that could change the microstructure. Salmi et al. established that a well-performing alternative to facilitate a correct heat flow preventing deformations caused by the material shrinkage is the use of support structures [18]. A considerably large body of literature proved that using suitable supports improves the densification behaviour and avoids the formation of cracks [19]. With the application of the appropriate support structures, Ahuja et al. successfully produced via PBF-LB\M Al-Cu alloys that are typically considered difficult to weld [20]. In addition, Liu et al. demonstrated as stable support structures not only prevent problems related to the extremely high PBF-LB\M cooling rate but also ensure proper sample-platform adhesion [21].

Although the issues related to residual stresses are embedded in the PBF-LB\M technique, the alloy composition can exacerbate crack and delamination phenomena [5]. Among the different parameters thermally involved in the additive process, a key role is played by the thermal conductivity coefficient (λ) of the chosen alloy. The AlSi10Mg, one of the widely used Al-based alloys in PBF-LB\M production, is characterised by a high thermal conductivity coefficient (130 $Wm^{-1}K^{-1}$) [22]. Based on the study conducted by Geng et al., a high thermal conductivity ensures a rapid heat transfer, uniform temperature distribution and efficient cooling during the additive process, and thus preventing thermally induced stresses and reducing crack sensitivity [23]. In addition, Liu et al. proved that the AlSi10Mg quasi-eutectic composition allows a reduced hot tearing sensitivity thanks to the small solidification range [24]. Although AlSi10Mg is suitable for the PBF-LB\M process, the addition of different alloying elements to improve its properties and heat stability remains an ongoing challenge [25]. The addition of Cu to the Al-based alloy has attracted wide interest in aerospace industries, in fact, these alloys represent the 45 % of the entire Al-alloys portfolio used in civil aircraft, as indicated in Wang et al. work [26]. Although adding 4 wt% Cu in AlSi10Mg has resulted in crack-free and full-dense samples in Martin et al. work, the addition of a larger amount of Cu has not yet been adequately explored in the literature [27]. Aksöz et al. proved that adding copper in Al-based alloys results in decreased thermal conductivity [28]. This reduction worsens heat diffusion during the PBF-LB\M and consequently increases the thermally induced stresses [29]. Moreover, another potentially detrimental effect of adding more copper than its solubility limit (5.05 wt%) in the aluminium matrix could result in an extension of the solidification range. Lu et al. proved that the extension of the solidification range leads to the appearance of hot tearing [30].

The aim of this work is to study a methodology that allows to processed via PBF-LB\M even the crack-prone Al-based compositions. In the present work, a new AlSi10Cu8Mg composition never processed by PBF-LB\M was chosen. This promising composition may exploit different strengthening mechanisms through the precipitation of the Al_2Cu phase and the supersaturated solid solution in the as-built condition. However, as previously reported, the decrease in the thermal conductivity coefficient and the increase of the solidification range due to the addition of 8 wt% Cu in AlSi10Mg could compromise the processability via PBF-LB\M. A rigorous study on the factors that could reduce crack formation and delaminations was conducted. Through the synergic use of different strategies, all delaminations were avoided and full-dense samples with high microhardness values were obtained.

2. Material ad methods

2.1. Powder characterisation

The AlSi10Cu8Mg powder was produced by our research group using PSI HERMIGA 100/10 VI VIGA gas atomiser starting from

AlSi10Mg and pure Cu ingots. A backfill operation was carried out before the vacuum induction melting (VIM) to avoid the evaporation of volatile elements. Considering the high oxidation tendency of the Al-based alloys, an inert high purity argon atmosphere was used during the gas atomisation process. The gas atomisation parameters were provided by the gas atomiser company PSI ltd. In addition, due to the high reactivity of the powder, the powder was passivated after gas atomisation to prevent explosivity problems. Before its characterisation, the powder was sieved between 20 and 50 μm as suggested for PBF-LB\M production. A scanning electron microscopy (SEM) analysis using Phenom XL was performed to determine the morphology of powder particles. The internal defects were indeed investigated through the Leica DMI 5000 M optical microscope on cross-sectioned powder. As observable in the micrograph of Fig. 1a, powder particles are almost spherical and with a limited number of satellites. The cross-sectioned particles revealed limited and small internal gas porosities (indicated with red arrows in Fig. 1b) resulting from the gas atomisation process. After an accurate image analysis on 20 images taken with the optical microscope, the internal porosity of the particles was calculated to be around 0.02 %. The particle size distribution was measured using a Mastersizer3000 laser diffraction particle size analyser and reported in Fig. 1c. The powder is characterised by D10, D50 and D90 values of 17.3, 28.8 and 45.6 μm, respectively.

Before the PBF-LB\M process, the sieved powder was dried in a drying oven at 90 °C for 2 h. According to Weingarten et al., the drying procedure markedly reduces gas pores after PBF-LB\M production [31].

2.2. PBF-LB|M production

The PBF-LB\M production was carried out in a Concept Laser Mlab cusing R equipped with a Gaussian beam fiber laser. The energy source was characterised by a maximum power of 100 W, a wavelength of 1070 nm and a laser spot of 50 μm. Argon was used as protective atmosphere. The PBF-LB\M system featured a build volume of 90 × 90 × 80 mm^3. To quickly define power (P), scan speed (v) and hatch distance (hd) values perspective for well-densified bulk samples, the single scan track (SST) method was exploited. SSTs were realised with a wide range of scan speed values (350–1400 mm/s) and three different power values (85, 90, and 95 W). An innovative algorithm implemented by Martucci et al. was used to perform an accurate SSTs analysis while avoiding operator error and subjectivity [32]. The algorithm discards unsuitable P-v combinations based on different SST quality indexes. Furthermore, by calculating the thickness of the SSTs obtained with the remaining P-v combinations and considering an overlapping of 0 % as recommended in Bosio et al. [33], the algorithm is able to calculate the most suitable hd value for the bulk production. The P, v and hd combinations not discarded by the software were used for the production of 10 × 10 × 10 mm^3 cubic samples. The layer thickness (l) was fixed at 15 μm as suggested by Concept Laser for the Al alloys. A chessboard scanning strategy with a rotation of 90° was used for the entire bulk production due to its efficiency in generating an isotropic stress tensor in the component after the PBF-LB\M process. All the parameters used for the bulk production are reported in Table 1 with the corresponding VED values calculated as reported in Equation (1).

$$VED = \frac{P}{l \cdot hd \cdot v} \quad (1)$$

To avoid delamination and crack formation, additional jobs were performed exploiting lower scan speed values and support structures. The geometry of the support structures was designed with an easy-to-vary and efficient configuration. Among the different geometries examined in the literature, a fully circular (conical and cylindrical) configuration was the most suitable for the present application. Han et al. previously exploited this support shape, demonstrating an excellent ability in anchoring overhang structures and an easy-to-model heat transmission [34]. The optimisation of support heights and diameters was carried out using cantilever parts. The support structure geometry that ensured a proper adhesion of the overhanging part and minimised the bending after cutting was chosen for the present study and reported in red in Fig. 2. On the other hand, as recommended by Liu et al., support structures with a larger contact area should be placed in the perimeter area of the cubes [21]. For this reason, supports with a fully cylindrical shape were placed along the sample perimeter (indicated in blue in Fig. 2).

In order to try to avoid delamination and crack formation, a synergic approach of strategies based on scan speed reduction and support use was applied. The process parameters explored for the bulk production with scan speed reduction were reported in Table 2.

2.3. Characterizations

After the PBF-LB\M process, the as-built specimens were removed from the platform using an electrical discharge machine. Firstly, the samples were analysed with a Leica EZ4 W stereomicroscope to obtain an overview of the macroscopic delaminations. To evaluate the densification level and possible internal cracks, all samples were cut along the building direction and polished using the standard metallographic procedure. When necessary, the samples were embedded in conductive resin before the cutting and polishing procedure. The densification level was evaluated with image analysis. Micrographs (100x magnification) covering the entire XZ section of the sample were taken with Leica DMI 5000 M optical microscope and then stitched together. Subsequently, the stitched image was processed

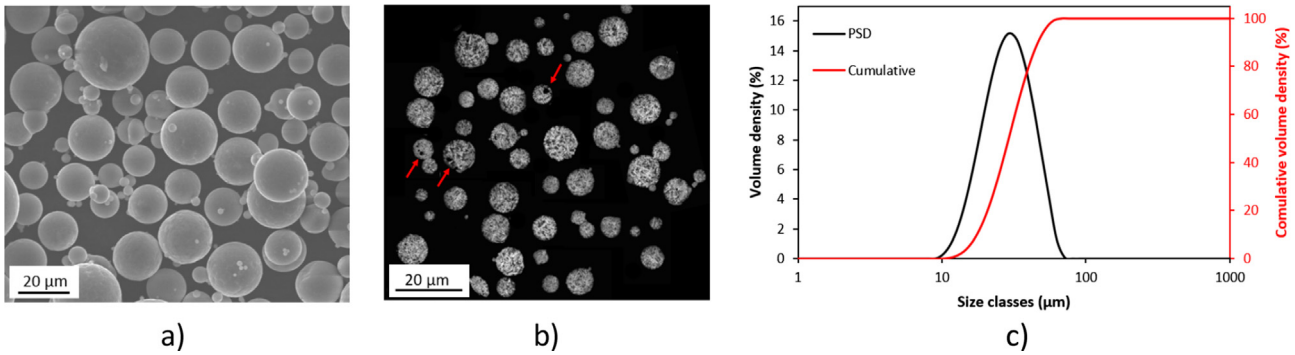

Fig. 1. Powder micrograph (a), optical image of the cross-sectioned powder (b) and particle size distribution (c) after sieving.

Table 1
Process parameters used for the bulk production.

P (W)	v (mm/s)	hd (μm)	l (μm)	VED (Jmm^{-3})	Scanning strategy
85	500	130	15	87.2	Chessboard strategy
85	650			67.0	
90	500			92.3	
90	650			71.0	
95	500			97.4	
95	650			95.0	

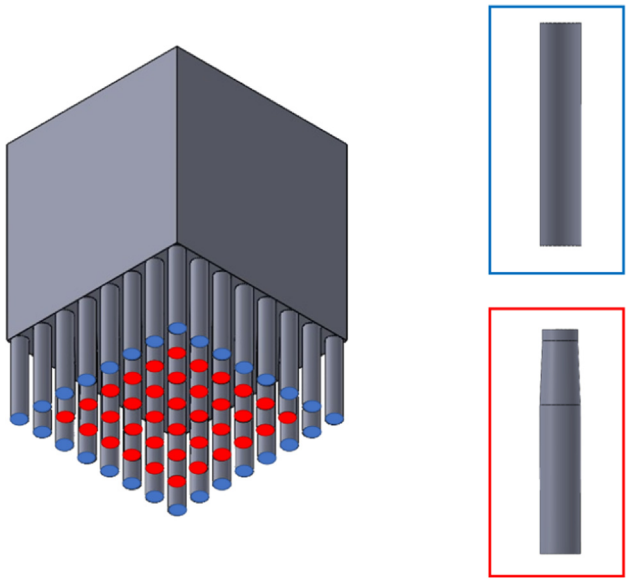

Fig. 2. Geometries of support structures and their location under the sample.

Table 2
Process parameters window exploited to avoid delamination formation.

P (W)	v (mm/s)	hd (μm)	l (μm)	VED (Jmm^{-3})	Scanning strategy
85	100	130	15	435.9	chessboard
	200			217.9	strategy
	300			145.3	
	400			109.0	
90	100	130	15	461.5	chessboard
	200			230.8	strategy
	300			153.8	
	400			115.4	
95	100	130	15	487.2	chessboard
	200			243.6	strategy
	300			162.4	
	400			121.8	

using ImageJ software, which is able to distinguish pores and cracks from the matrix after thresholding and thus calculate the relative density. The homogeneous distribution of the alloying elements was verified by EDS analysis using ZEISS EVO 15 SEM. Finally, a microhardness test was performed using a Vickers tester VMHT Leica according to ASTM E384 standard. Ten microhardness indentations were performed on the XZ plane using a static load of 0.5 kg and a dwell time of 10 s.

3. Results and discussion

3.1. Problem statement

In order to rapidly approach a narrow process parameter window for the bulk production, the SST method was used. Among

Fig. 3. SST parameters explored for the first screening. The SSTs with strong discontinuities are reported in red and SSTs with low quality are marked in orange. (For interpretation of the references to colour in this figure legend, the reader is referred to the web version of this article.)

others, Aversa et al. demonstrated that the SST method allows the P-v combinations that are more compatible with good bulk densification to be correctly predicted [35]. With this fast method, a wide range of P-v combinations was explored and the parameters not able to guarantee an adequate bulk densification were rapidly discarded by a software previously developed by the authors. Fig. 3 reports the full spectrum of SST parameters analysed as located on the platform and their corresponding P-v values. In particular, the conditions in which SSTs with strong discontinuities were obtained are marked in red and the conditions with low quality indexes are indicated in orange. The selected P-v combinations and the hd value calculated by the software were then used for cube production (Table 1).

As observable in Fig. 4, unpredicted delaminations occurred when cubic samples were produced with the parameters suggested by the SST software.

The delamination formation can be attributed to several factors: the non-homogeneous dispersion of the alloying elements, significant defects (such as lack of fusion and pores) or stresses generated during the additive process. In order to investigate the origin of delamination, the samples were observed with stereomicroscope, optical microscope and SEM in backscattered mode. As no microstructural differences were revealed among all samples, only one representative sample was reported in Fig. 5. Delaminations are always perpendicular to the build direction (Z), start from the outer surface of the sample and generally pass through the entire section. Observing the high-magnification micrographs of cracks in Fig. 5, it is not possible to state any correlation between delamination and sample defects. In particular, the optical analysis did not reveal any copper clusters, inhomogeneities or defects in crack areas. Otherwise, the SST software would not suggest the related process parameters. In fact, the strength of the SST system lies in avoiding parameters that would lead to defects such as lack of fusion or keyhole pores.

Furthermore, the volumes between delaminations appear free from cracks and show minimal gas porosity. The mean relative

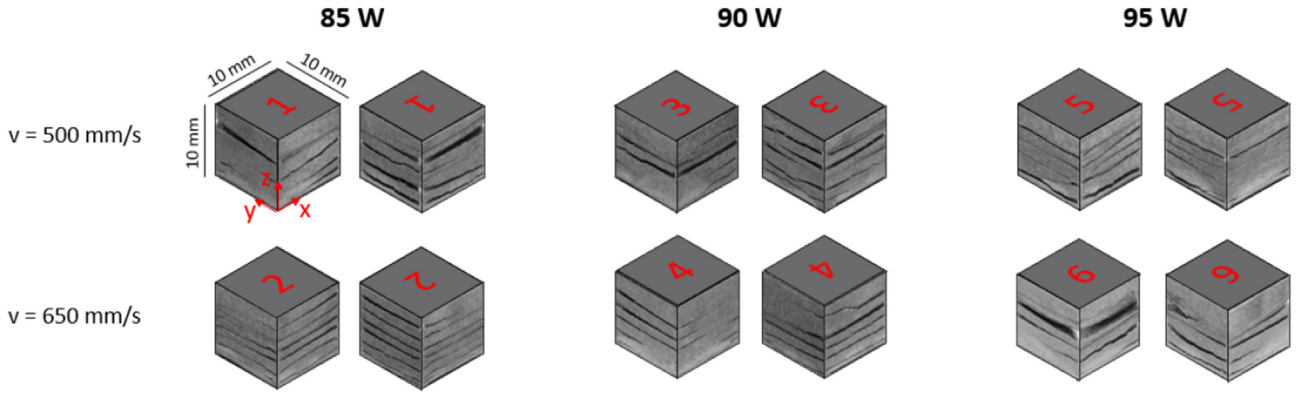

Fig. 4. Visual reconstruction of all faces of the samples produced with process parameters indicated by the SST software.

density of the densified foils evaluated by image analysis on XZ plane of all samples was 99.1 %.

After excluding potential causes of the delamination formation related to microstructural features, the attention was focused on the stresses generated during the additive process. As well explored in Mercelis et al. work [36] and represented in Fig. 6, in the PBF-LB\M technique two mechanisms of residual stress formation occur throughout the process. The first phenomenon is derived from the extremely high temperature caused by the laser passage (Fig. 6a). The laser passage involves not only the last powder layer melted (l_n) but also the layers below. In the present discussion, the last melted layer, l_n, and the solidified layers thermally involved by the laser passage is identified as the "warm volume" for the sake of simplicity. During the laser passage, the warm volume tends to expand due to its high temperature, but this expansion is constrained by the previously-solidified volume below. This phenomenon generates compressive stresses (σ_C) in the interface layers (the layers between the warm volume and the previously-solidified volume below). If the generated stresses exceed the yield strength of the material, plastic deformations occur. The second mechanism regards residual stresses generated during the cooling phase of the warm volume (Fig. 6b). The latter, during the cooling phase, tends to shrink but the contraction is again limited by the previously-solidified volume below. This phenomenon results in tensile stresses (σ_T) that cause plastic deformations in interface layers. In addition, the deformations induced by the phenomena explained above are proportional to the temperature gradient according to Equation (2).

$$\varepsilon = \alpha \Delta T \tag{2}$$

where ε indicates the deformation, α the thermal expansion coefficient and ΔT the thermal gradient. The thermal gradient in turn depends on the high temperature reached in the warm volume and the thermal conductivity of the previously-solidified volume below that controls its temperature. The greater the thermal gradient, the greater the deformations induced and thus the stresses according to Hooke's law. The PBF-LB\M process is a cold process and it is typically characterised by a high thermal gradient between the warm volume and the previously-solidified volume. Consequently, based on the material properties (α, λ, Young's Modulus), significant stresses are induced in the final component. In addition, a key role is played by the elongation at the break of the material. In fact, the lower the elongation at the break of the material, the less plastic deformation the material can undergo before irreversible crack nucleation. The layer-by-layer melting and the solidification with extremely high rates subject the material to rapid heating–cooling cycles and thus to rapid crack propagation. Based on Hussein et al. simulations [37], the thermal evolution of l_n during its scanning and the scanning of the subsequent i-layers was reported in Fig. 6c. The i-layers are the set of layers that, when scanned, thermally affect the layer l_n. Consistent with the thermal cycling and the phenomena described above, the stress profiles to which the inter-

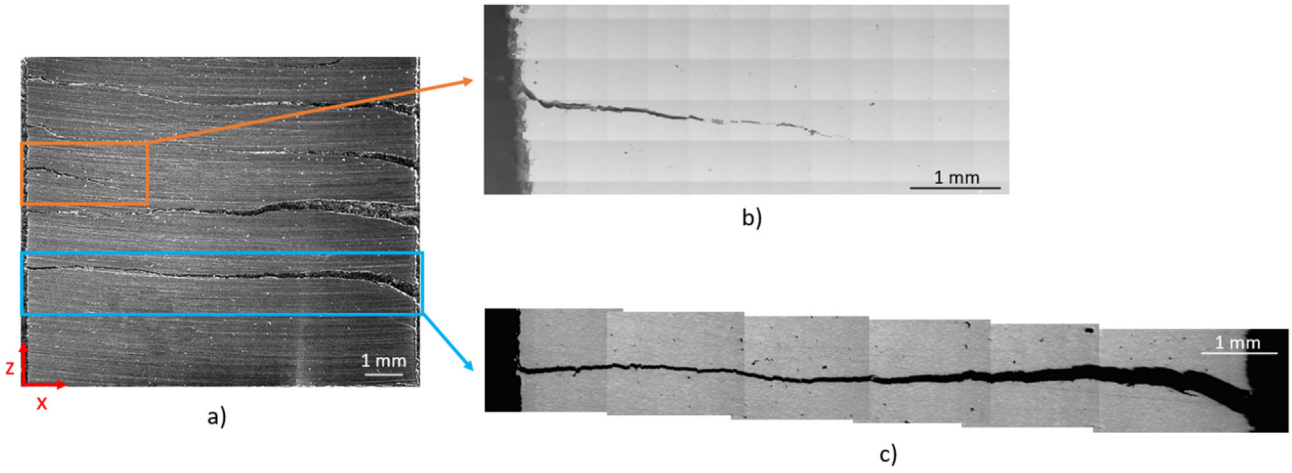

Fig. 5. Image of a representative sample taken with a stereomicroscope (a) and detailed micrographs of cracks taken using SEM in backscattered mode (b) and optical microscope (c).

face layers are subjected were plotted (Fig. 6c). It is important to emphasise that the thermal cycle undergone by l_n occurs in order of ds. The rapid cyclic repetition of the above-mentioned phenomena can thus be perceived as thermal fatigue.

The issues resulting from the phenomena illustrated in Fig. 6 can be exacerbated by the cracking tendency of some alloys, such as the AlSi10Cu8Mg analysed in this work. Based on Aksöz et al. study on the Al-Cu binary system [28], it is reasonable to assume that the thermal conductivity will be reduced by adding 8 wt% Cu to the AlSi10Mg system. Lower thermal conductivity worsens heat transfer by not allowing rapid heat homogenisation, thus inducing higher residual plastic deformation and increasing the cracking tendency.

To minimise the thermally induced stresses resulting from the PBF-LB\M process, different methods were exploited in the literature. For example, Kempen et al. minimised delaminations occurring during the processing of M2 High-Speed Steel alloy by lowering thermal gradients and thus increasing the temperature of the previously-solidified volume through platform heating [16]. However, the use of platform heating on the composition analysed in the present work would be problematic as the first precipitation phenomena occur at around 147 °C (as demonstrated by the DSC spectrum in Fig. A1) and the temperatures that ensure a reduction in crack formation are usually over 150 °C. For this reason, other methodologies to avoid delamination formation were considered.

3.2. Effects of the process parameters

Several process parameters are involved during PBF-LB\M production, but the strongest influence in stress formation is provided by scanning strategy, scan speed, and VED. In the present work, a chessboard scanning strategy with a rotation of 90° was exploited for the bulk production in order to minimise the residual stresses induced in the component. As proved by Zaeh et al., the chessboard scanning strategy have a strong impact on residual stress reduction thanks to shorter scan vectors [38]. After fixing the scanning strategy for the bulk production, the effect of scan speed value on the residual stress and thus on delamination was investigated. As demonstrated by Vasinonta et al., with a slow laser scan speed, residual stresses can be powerfully reduced [39]. This reduction can be attributed to the reduced temperature gradients according to Vasinonta et al. [40] and the decreased cooling rate according to Manvatkar et al. [41]. In the present work, four scan speed val-

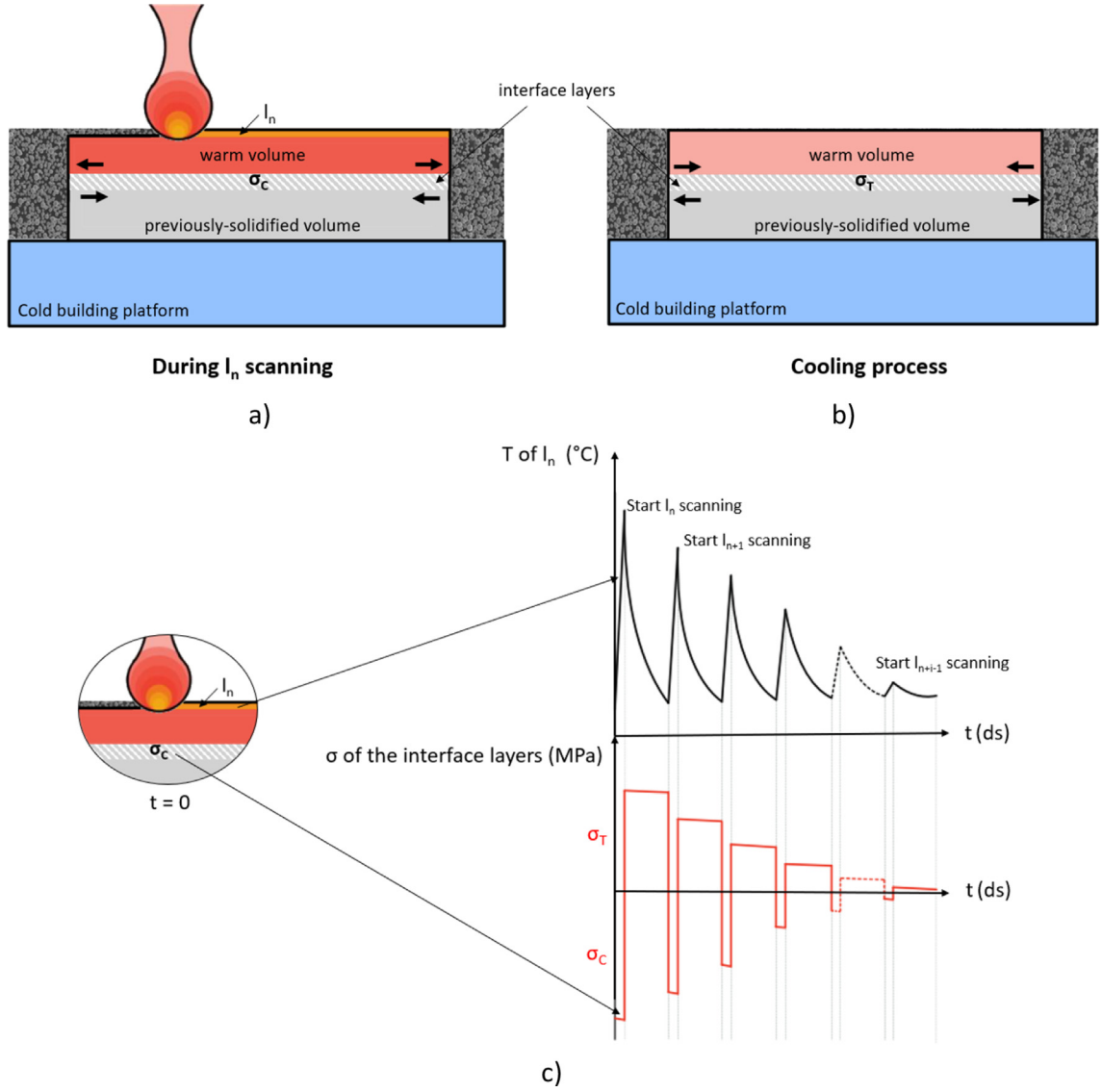

Fig. 6. Mechanisms of residual stress formation occurring during scanning phases (a) and cooling phases (b) in the PBF-LB\M process. The thermal evolution of l_n during its scan and successive scans was reported in (c) with the corresponding stresses induced in the interface layers.

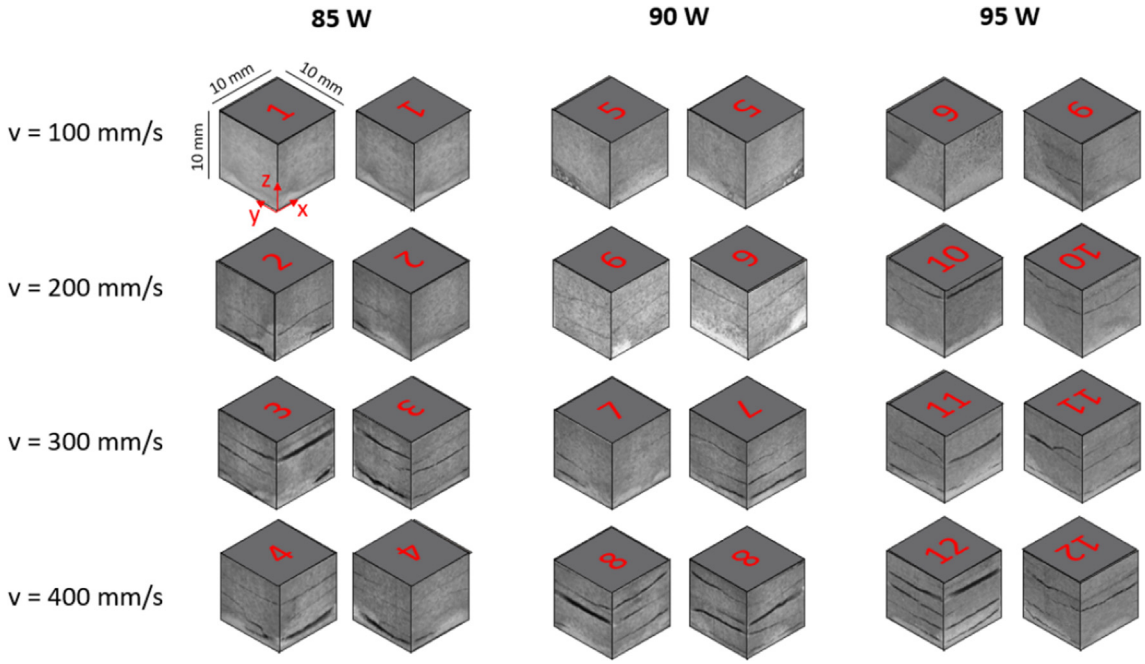

Fig. 7. Visual reconstruction of all faces of the samples produced by reducing the scan speed values.

ues (400, 300, 200 and 100 mm/s) and the three power values (85, 90 and 95 W) previously investigated were further explored for the bulk production. The reconstruction of the samples obtained is displayed in Fig. 7.

Observing Fig. 7, the delamination formation seems not highly power sensitive but strongly influenced by the scan speed. From 400 to 100 mm/s, a strikingly reduction of 65 % in the number of delaminations was highlighted regardless of power values used. The samples with fewer and smaller cracks are the ones produced at 100 mm/s. In order to better analyse these samples, the visual examination was performed again by removing the sample skin. Then, XZ cross-sections of the samples produced with scan speed of 100 mm/s were observed with the stereomicroscope to evaluate the internal densification. The results are displayed in Fig. 8.

Observing Fig. 8, the correlation between laser power and delamination formation becomes clearer. Samples built with a power value of 85 W exhibit delaminations throughout the entire sample cross-section. Whereas, when the power value is above 85 W, only cracks without through delaminations can be detected. Otherwise, the only use of lower scan speed did not allow the complete elimination of cracks regardless of the power value.

3.3. Influence of support structures

As explained in Fig. 6, the residual stresses responsible for the formation of cracks result from an extreme thermal gradient between the warm volume and the previously-solidified volume below. Based on these considerations, a slowdown in heat flow could have favourable effects on sample densification. A successful strategy to reduce the heat flow is the application of support structures between the cold build plate and the component to be built. There is a large volume of published studies describing the role of

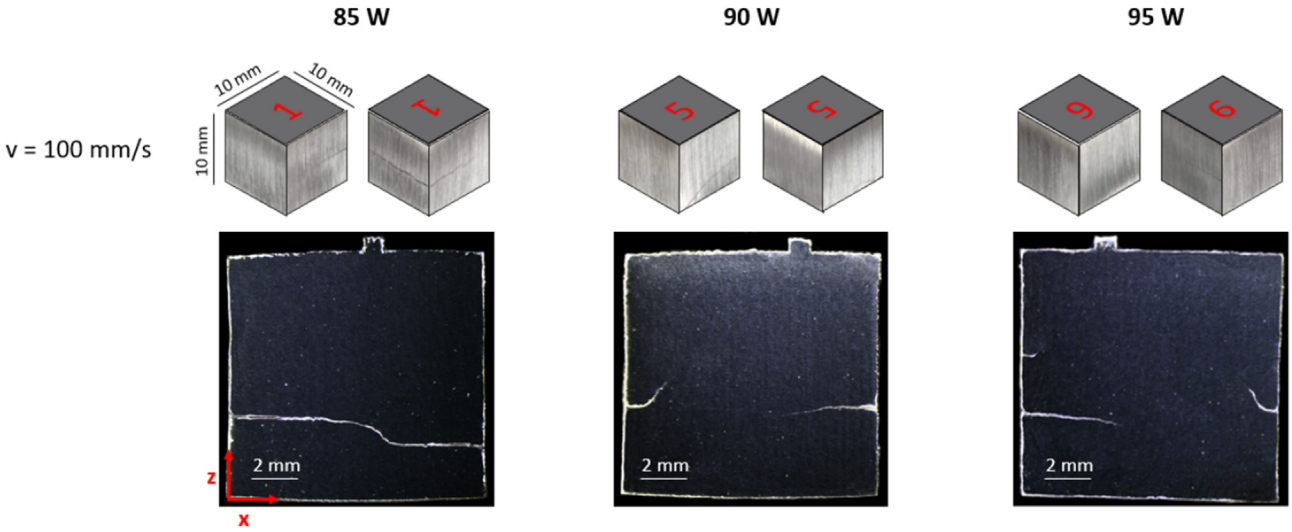

Fig. 8. Visual reconstruction of samples produced with the slowest scan speed and the corresponding XZ cross-sections observed with the stereomicroscope.

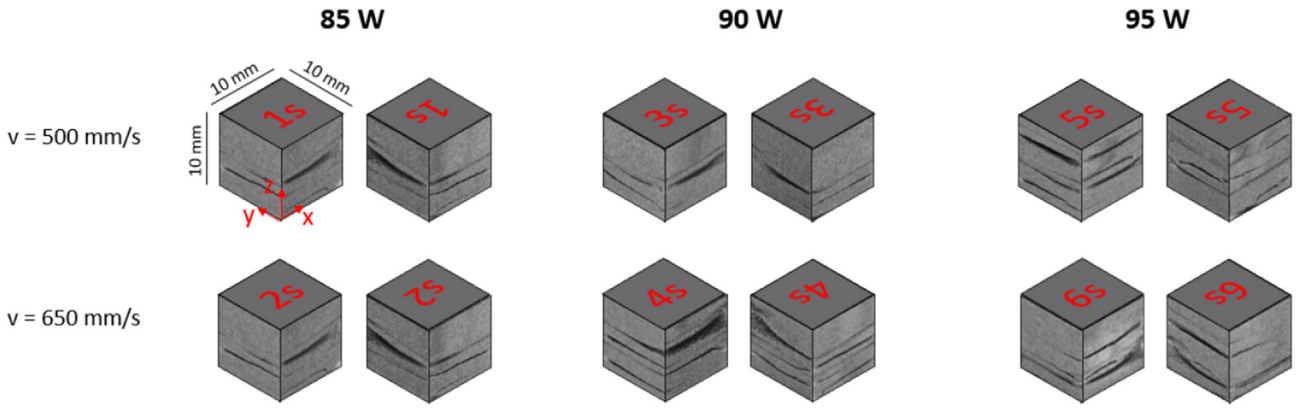

Fig. 9. Visual reconstruction of all faces of the samples produced with process parameters indicated by SST software and support structures.

support structures in more efficient densification as mentioned in the introduction. To investigate the effect of the support structures on AlSi10Cu8Mg processability, the parameters suggested by the analysis of the SSTs (Table 1) were used also to produce cubic samples with supports. The results are reported in Fig. 9.

Notwithstanding the application of support structures, delamination phenomena again occurred in the samples built with power values of 85 – 90 – 95 W and scan speeds of 500 and 650 mm/s. However, comparing the samples obtained using the same parameters with and without supports (Fig. 4 and Fig. 9), it is possible to note a 50 % decrease in full-section delaminations. This reduction can be attributed to a different heat conduction along the build direction, in line with Zhang et al. work [42]. Firstly, samples without supports have an exchange surface toward the platform equal to its section, while the exchange section is limited when the support structures are applied. Secondly, supports are surrounded by the unmelted powder, that is interpose between the sample base and the platform. In this case, it is reasonable to assume that the previously-solidified volume maintains a higher temperature because the heat conduction during the process changes being the powder bed thermal conductivity-one order of magnitude lower than that of the bulk, as demonstrated in Li et al. work [43].

In order to avoid delamination and crack formation, a synergic approach of strategies based on scan speed reduction and support use was applied. The results are displayed in Fig. 10.

Although minimal cracks are still visible at low power, the use of both a lower scan speed and supports resulted in a cracks-free sample with the maximum power (95 W).

It is important to emphasise that the cracking phenomenon is dependent on the size and shape of the sample produced [44]. As the described phenomena are strongly affected by layer-by-layer scanning, a much higher number of scans or very large part cross-sections would expose the sample to higher thermally induced stresses and thus require further parameter optimisation [21]. The process parameters and geometry of the support structures used in this work are closely related to the type of sample produced. However, this work aimed to develop a practical approach to conduct a systematic study of the processability of a highly crack-sensitive alloy such as AlSi10Cu8Mg, which was successfully achieved.

3.4. Investigations of microstructural and mechanical features

When the optimal processing conditions to produce crack-free samples of AlSi10Cu8Mg were found, preliminary sample microstructural and mechanical features were evaluated.

In order to exclude the presence of cracks, a complete XZ cross-section of the sample was observed through an optical microscope. With the OM it is, in fact, possible to create a stitched version of images taken on the entire sample. From the stitched image

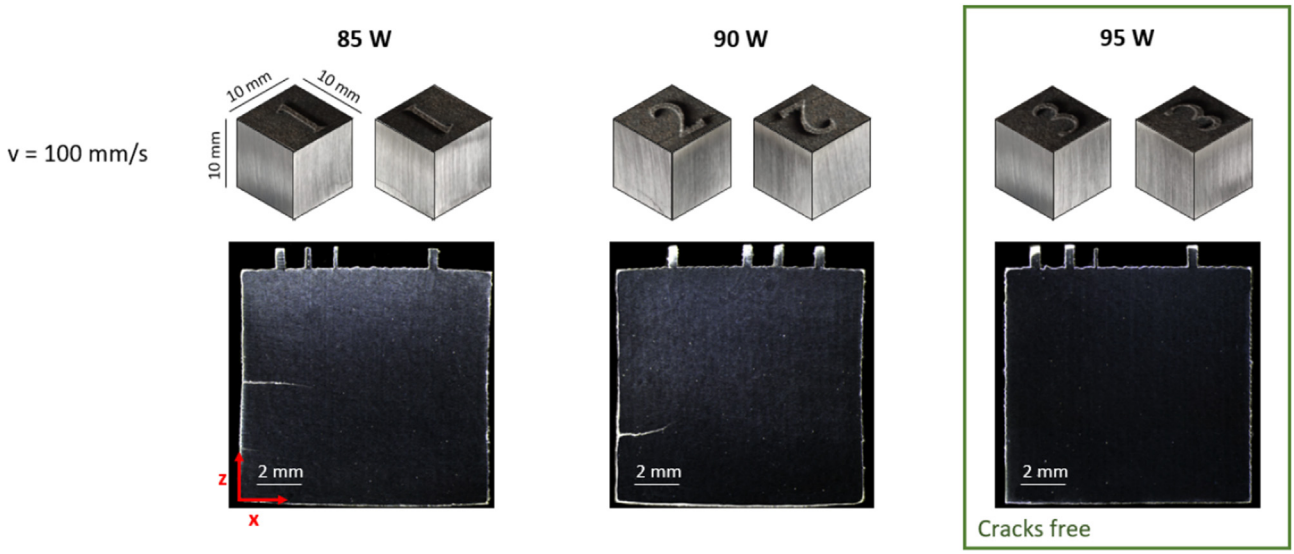

Fig. 10. Visual reconstruction of samples produced at 100 mm/s with support structures and the corresponding XZ cross-sections observed with the stereomicroscope.

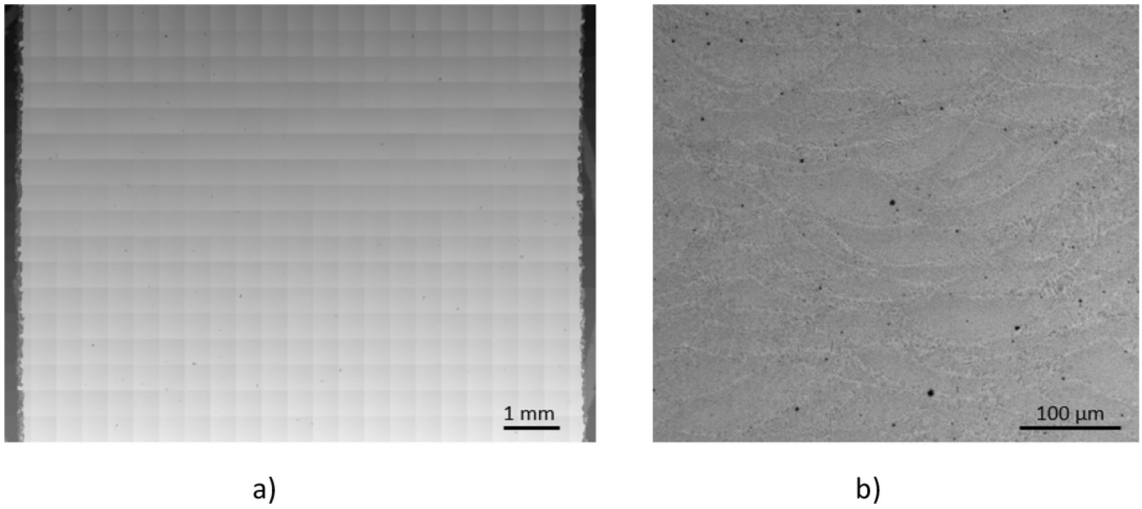

Fig. 11. A stitched image of the XZ section of the sample and higher magnification micrography.

reported in Fig. 11a, it is possible to exclude the presence of any minor cracks. Using all the OM images taken, the relative density of the sample was evaluated through ImageJ software. The obtained relative density was 99.8 %, with a standard deviation of 0.2. In particular, observing the micrograph in Fig. 11b, only a few small gas porosities can be detected. The term 'gas porosity' is usually used to refer to spherical porosities that are not located in a particular position in the melt pool. The origin of these porosities can be traced to the moisture in the powders, the gas trapped in the particles after gas atomisation and the dynamics of the PBF-LB\M process. As suggested by Weingarten et al. [31], in the present work the powders were dried immediately before the additive process to remove surface moisture and thus limit the formation of gas porosities. In addition, by optimising the gas atomisation process it was possible to minimise the amount of gas-trapped particles produced, as can be seen from the micrograph in Fig. 1b where the porosity of the particles was calculated to be around 0.02 %. This suggests that gas-trapped powder particles cannot fully account for the gas porosities found in the bulk sample, however, the dynamics of the PBF-LB\M process can explain it. Due to the PBF-LB\M process taking place in an inert atmosphere, the powder stream traps the protective gas (argon). The latter enters the melt pool through the Marangoni's flow, which tends to retain entrapped gas bubbles. Notwithstanding, considering the low porosity and the geometrical features of this type of porosity, they should not be considered detrimental to mechanical performance.

Preliminarily, the mechanical behaviour of the AlSi10Cu8Mg was analysed through a Vickers microhardness test on a plane parallel to the build direction. A mean microhardness of 190 HV was obtained with a standard deviation of 2 HV. It can be seen that this composition achieved higher microhardness values than those recorded by Kempen et al. on the pure AlSi10Mg alloy (127 HV) and by Martin et al. on the gas atomiser AlSi10MgCu4 system (156 HV) [27,44]. As well explained in Ashby et al., the microhardness is related by a factor of 1/3 to the yield strength of the material [46]. For this reason, it can be stated that the AlSi10Cu8Mg alloy is characterised by a significantly higher yield strength value than the AlSi10Mg system and AlSi10MgCu4. This improvement could be explained by the combined effect of strengthening due to Cu in solid solution and strengthening due to the precipitation of the Al_2Cu phase. It is reasonable to assume that variations in the local cooling rate, temperature gradient and heat accumulated during the PBF-LB/M process may result in non-homogeneous microstructure along the sample height and, thus, consistently dif-

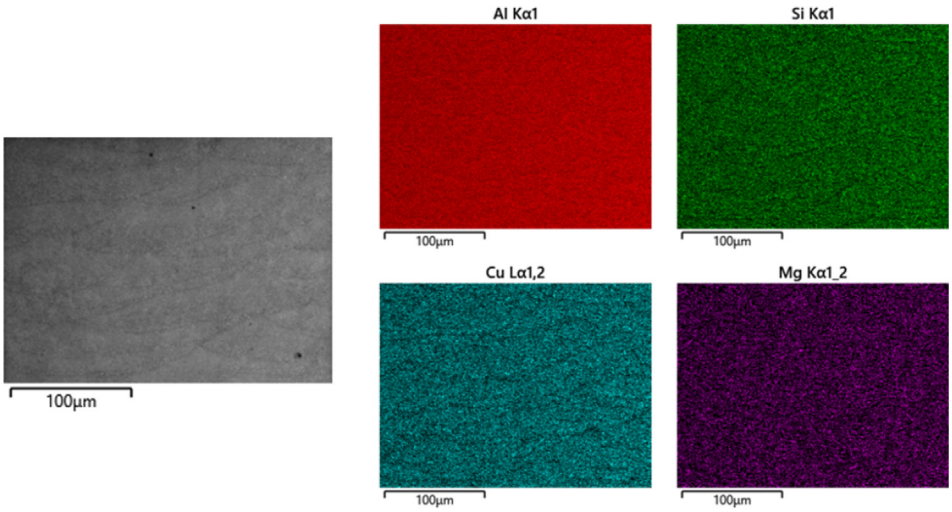

Fig. 12. The selected area for EDS maps and the corresponding Al, Si, Cu and Mg distributions.

ferent mechanical properties. However, these assumptions lapsed after conducting microhardness measurements along the growth direction and noticing a minimal standard deviation. The latter suggests that, under the sample size analysed and the process conditions used, the sample microhardness is not strongly affected by these factors and is reasonably homogeneous along the growth direction. An EDS analysis performed with SEM verified the correct homogenisation of the alloying elements at a micrometre scale, excluding the detrimental presence of copper clusters (Fig. 12). Further investigations into the microstructure failures and advanced mechanical properties of this promising alloy will be part of future studies.

4. Conclusions

A growing body of literature is increasingly focusing on the development of new alloys tailored for PBF-LB\M production. The goal is to obtain high-strength, lightweight alloys with a high level of densification. The preference often falls on aluminium-based alloys due to their convenient strength-to-weight ratio. Although the processability of high strength Al alloys is of industrial and research interest, it is severely limited by their high cracking tendency. For example, emerging compositions in PBF-LB\M production were obtained by adding Cu to AlSi10Mg. However, these kinds of compositions explored so far do not exceed 4 wt% Cu as this would drastically increase the cracking tendency. In order to define some strategies to make no standard compositions processable via PBF-LB\M, in the present work the pre-alloyed composition AlSi10Cu8Mg was chosen. The approach adopted for processing and the results obtained were summed up below:

- The use of the SST method led to discarding P-v combinations unsuitable for PBF-LB\M processing;
- The P-v combinations suggested by the SST method with the calculated hd were used as starting point for the production of cubes. However, these conditions, while leading to high material density, proved to be unsuitable for bulk processing as they resulted in undesirable delaminations;
- Decreasing the scan speed resulted in an approximately 65 % reduction in the occurrence of through-section delaminations although, a proper densification of the samples could not be achieved;
- Using the parameters resulting from the SSTs analysis, with the application of support structures a drastic reduction of 50 % in through-section delaminations was achieved;
- Only the synergetic use of low scan speeds, suitable laser powder values and support structures resulted in a crack-free and fully-dense specimen. In particular, the sample produced with the optimised process conditions showed a densification of 99.8 % and no crack.
- Investigation of the mechanical properties resulted in very high microhardness values on the sample cross-section with an average value of 190 HV (+48 % compared to AlSi10Mg and + 22 % compared to AlSi10MgCu4).

In this work, it was demonstrated that the synergetic use of scan speed reduction and the use of support structures enables efficient processing of cracking-sensitive alloys, even when no platform heating is permitted. The efficient methodology used in the present work to quickly define process conditions without crack and delamination formation can be extended to all new compositions affected by cracking tendency. This methodology establishes a new step in expanding the materials portfolio of the PBF-LB\M process.

Data availability

Data will be made available on request.

Declaration of Competing Interest

The authors declare that they have no known competing financial interests or personal relationships that could have appeared to influence the work reported in this paper.

Acknowledgements

A special acknowledgement goes to Enrico Virgillito, who contributed to the powder gas atomisation.

Appendix

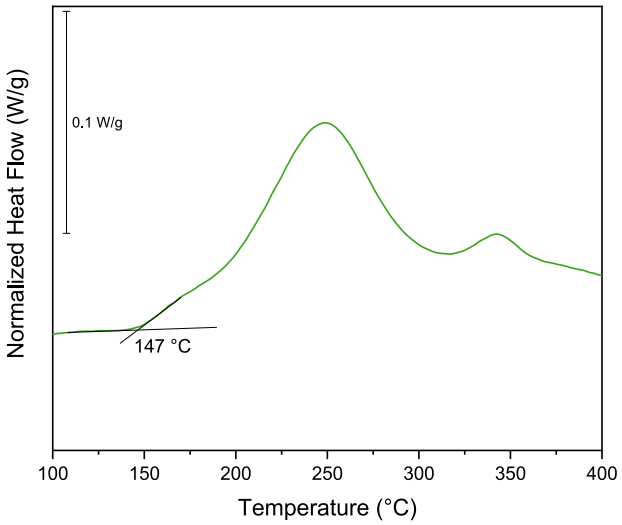

Fig A1. DSC of an AlSI10Cu8Mg as built sample

References

[1] M. Avateffazeli et al., Correlation between tensile properties, microstructure, and processing routes of an Al–Cu–Mg–Ag–TiB2 (A205) alloy: additive manufacturing and casting, Mater. Sci. Eng. A 841 (2022) 142989.
[2] Y. Zhao et al., A comparative analysis of Inconel 718 made by additive manufacturing and suction casting: microstructure evolution in homogenization, Addit. Manuf. 36 (2020) 101404.
[3] S. Dadbakhsh, L. Hao, Effect of Al alloys on selective laser melting behaviour and microstructure of in situ formed particle reinforced composites, J. Alloy. Compd. 541 (2012) 328–334.
[4] C. Chen et al., Residual stress of typical parts in laser powder bed fusion, J. Manuf. Process. 59 (2020) 621–628.
[5] H. Hyer et al., Composition-dependent solidification cracking of aluminum-silicon alloys during laser powder bed fusion, Acta Mater. 208 (2021) 116698.
[6] A. Staub, A.B. Spierings, K. Wegener, Correlation of meltpool characteristics and residual stresses at high laser intensity for metal lpbf process, Adv. Mater. Processing Technol. 5 (1) (2019) 153–161.
[7] Q. Han et al., Laser powder bed fusion of Hastelloy X: effects of hot isostatic pressing and the hot cracking mechanism, Mater. Sci. Eng. A 732 (2018) 228–239.
[8] X. Jiang, T. Ye, Y. Zhu, Effect of process parameters on residual stress in selective laser melting of AlSi10Mg, Mater. Sci. Technol. 36 (3) (2020) 342–352.
[9] Kruth, Jean-Pierre, et al. "Assessing and comparing influencing factors of residual stresses in selective laser melting using a novel analysis method." Proceedings of the institution of mechanical engineers, Part B: Journal of Engineering Manufacture 226.6 (2012): 980-991.

[10] L. Parry, I.A. Ashcroft, R.D. Wildman, Understanding the effect of laser scan strategy on residual stress in selective laser melting through thermo-mechanical simulation, Addit. Manuf. 12 (2016) 1–15.
[11] D. Koutny et al., Influence of scanning strategies on processing of aluminum alloy EN AW 2618 using selective laser melting, Materials 11 (2) (2018) 298.
[12] M. Guo et al., Microstructure, mechanical properties and residual stress of selective laser melted AlSi10Mg, J. Mater. Eng. Perform. 28 (11) (2019) 6753–6760.
[13] H.u. Zhang et al., Selective laser melting of high strength Al–Cu–Mg alloys: processing, microstructure and mechanical properties, Mater. Sci. Eng. A 656 (2016) 47–54.
[14] J. Deng et al., Densification, microstructure, and mechanical properties of additively manufactured 2124 Al–Cu alloy by selective laser melting, Materials 13 (19) (2020) 4423.
[15] N.C. Levkulich et al., The effect of process parameters on residual stress evolution and distortion in the laser powder bed fusion of Ti-6Al-4V, Addit. Manuf. 28 (2019) 475–484.
[16] K. Kempen et al., Selective laser melting of crack-free high density M2 high speed steel parts by baseplate preheating, J. Manuf. Sci. Eng. 136 (2014) 6.
[17] D. Buchbinder et al., Investigation on reducing distortion by preheating during manufacture of aluminum components using selective laser melting, J. Laser Appl. 26 (1) (2014) 012004.
[18] A. Salmi et al., Experimental analysis of residual stresses on AlSi10Mg parts produced by means of Selective Laser Melting (SLM), Procedia Cirp 62 (2017) 458–463.
[19] Mishurova, Tatiana, et al. "The influence of the support structure on residual stress and distortion in SLM Inconel 718 parts." Metallurgical and materials transactions A 49.7 (2018): 3038-3046.
[20] B. Ahuja et al., Fabrication and characterization of high strength Al-Cu alloys processed using laser beam melting in metal powder bed, Phys. Procedia 56 (2014) 135–146.
[21] Y. Liu, Y. Yang, D.i. Wang, A study on the residual stress during selective laser melting (SLM) of metallic powder, Int. J. Adv. Manuf. Technol. 87 (1) (2016) 647–656.
[22] R.RJ. Sélo et al., On the thermal conductivity of AlSi10Mg and lattice structures made by laser powder bed fusion, Addit. Manuf. 34 (2020) 101214.
[23] S. Geng et al., Comparison of solidification cracking susceptibility between Al-Mg and Al-Cu alloys during welding: a phase-field study, Scr. Mater. 150 (2018) 120–124.
[24] J. Liu, P. Zeng, S. Kou, Solidification cracking susceptibility of quaternary aluminium alloys, Sci. Technol. Weld. Join. 26 (3) (2021) 244–257.
[25] K. Riener et al., Processability of high-strength aluminum 6182 series alloy via laser powder bed fusion (LPBF), Int. J. Adv. Manuf. Technol. (2022) 1–15.
[26] J.G. Wang, Z.T. Wang, Advance on wrought aluminium alloys used for aeronautic and astronautic industry (1), Light alloy fabrication technol. 41 (8) (2013) 1–6.
[27] A. Martin et al., Effect of the heat treatment on the microstructure and hardness evolution of a AlSi10MgCu alloy designed for laser powder bed fusion, Mater. Sci. Eng. A 819 (2021) 141487.
[28] S. Aksöz et al., Dependency of the thermal and electrical conductivity on the temperature and composition of Cu in the Al based Al–Cu alloys, Exp. Therm.. Fluid Sci. 34 (8) (2010) 1507–1516.
[29] C. Zhang et al., Thermal conductivity of Al–Cu–Mg–Si alloys: experimental measurement and CALPHAD modeling, Thermochim. Acta. 635 (2016) 8–16.
[30] R. Lu et al., Composition design method of Al-Cu alloy for laser powder bed fusion, J. Alloy. Compd. 914 (2022) 165298.
[31] C. Weingarten et al., Formation and reduction of hydrogen porosity during selective laser melting of AlSi10Mg, J. Mater. Process. Technol. 221 (2015) 112–120.
[32] A. Martucci et al., An automatic on top analysis of single scan tracks to evaluate the laser powder bed fusion building parameters, Materials 14 (18) (2021) 5171.
[33] F. Bosio et al., A time-saving and cost-effective method to process alloys by Laser Powder Bed Fusion, Mater. Des. 181 (2019) 107949.
[34] Q. Han et al., Manufacturability of AlSi10Mg overhang structures fabricated by laser powder bed fusion, Mater. Des. 160 (2018) 1080–1095.
[35] A. Aversa et al., Single scan track analyses on aluminium based powders, J. Mater. Process. Technol. 255 (2018) 17–25.
[36] Mercelis, Peter, and Jean-Pierre Kruth. "Residual stresses in selective laser sintering and selective laser melting." Rapid prototyping journal (2006).
[37] Hussein, Ahmed, et al. "Finite element simulation of the temperature and stress fields in single layers built without-support in selective laser melting." Materials & Design (1980-2015) 52 (2013): 638-647.
[38] M.F. Zaeh, G. Branner, Investigations on residual stresses and deformations in selective laser melting, Prod. Eng. 4 (1) (2010) 35–45.
[39] Vasinonta, Aditad, Jack Beuth, and Michelle Griffith. "Process maps for controlling residual stress and melt pool size in laser-based SFF processes 200." 2000 International Solid Freeform Fabrication Symposium. 2000.
[40] Vasinonta, Aditad, Jack L. Beuth, and Michelle Griffith. "Process maps for predicting residual stress and melt pool size in the laser-based fabrication of thin-walled structures." (2007): 101-109.
[41] V. Manvatkar, A. De, T. DebRoy, Spatial variation of melt pool geometry, peak temperature and solidification parameters during laser assisted additive manufacturing process, Mater. Sci. Technol. 31 (8) (2015) 924–930.
[42] S. Zhang et al., On thermal properties of metallic powder in laser powder bed fusion additive manufacturing, J. Manuf. Process. 47 (2019) 382–392.
[43] E.L. Li et al., A three-phase model for simulation of heat transfer and melt pool behaviour in laser powder bed fusion process, Powder Technol. 381 (2021) 298–312.
[44] R.K. Everett et al., A variogram analysis of build height effects in an additively manufactured AlSi10Mg part, Addit. Manuf. 35 (2020) 101306.
[45] K. Kempen et al., Mechanical properties of AlSi10Mg produced by selective laser melting, Phys. Procedia 39 (2012) 439–446.
[46] Ashby, Michael F., Hugh Shercliff, and David Cebon. Materials. engineering, science, processing and design. Butterworth-Heinemann, 2018.